ICAS 2016
30th Congress of the International Council of the Aeronautical Sciences
DCC, Daejeon, Korea ; September 25-30, 2016

DETAILED AERO-STRUCTURAL DESIGN OF WINGLET FOR BUSINESS JET

Nicolas R. El Haddad, Luis Gonzalez
Embry-Riddle Aeronautical University
elhaddan@my.erau.edu, gonzall8@erau.edu

Keywords: *design, aerodynamics, winglets, performance, structures*

Abstract

The aerodynamic design of a winglet for the Dassault Falcon 10 business jet was carried out. The design space was explored through vortex lattice method models, calibrated with respect to wind tunnel data. The best configuration was then analyzed with RANS and a finite element model of the original wing box was created (validated with respect to test data) to determine the weight penalty that the structural reinforcement due to the new loads would require.
The aircraft performance was then calculated and compared to the baseline aircraft. Net drag reductions of 4.8% at Mach 0.7 and 2.5% at Mach 0.8 were found. The range was increased by 66 NM (4.3%) and for a 1,200 NM mission, fuel burn was reduced by 3.9%.

1 Introduction

The Dassault Falcon 10 is a light business jet that can carry four passengers 2,000 NM, flying at Mach 0.75 at 35,000 ft, without fuel reserves. It has a maximum takeoff weight of 18,300 lb, a maximum operating Mach number of 0.87 and a 45,000 ft ceiling [1]. A total of 226 Falcon 10s and Falcon 100s (a variant) were produced between 1973 and 1989, of which about 200 are still active today [2].

For these aircraft, a retrofit winglet is an attractive option because due to drag reductions, without significant weight penalties, range and cruise speed could be increased; and, fuel burn, takeoff distances and takeoff noise could be decreased.

As a winglet span increases, the induced drag is reduced proportionally but the viscous and, or the wave drag and the structural weight will increase, possibly negating the performance improvement or resulting detrimental.

Various wingtip devices have been proposed and implemented, such as blended winglets [3], split winglets [4], downward winglets [5], C-shaped wing tips [6], raked wingtips, tip fences [7], tip sails [8], etc. For retrofitting into an existing airframe, the most straightforward are the blended winglets, the type that will be studied here.

The relative influence of the winglet geometrical parameters has already been studied [9] and it was shown that the most significant are the cant and sweep angles and the winglet span. In general, larger winglets achieve higher induced drag reductions but at the expense of increased friction drag and higher bending moments. High cant angles lead to increased aerodynamic interference (higher wave drag). However, they generate lower root bending moments (lower weight penalties). Conversely, low cant angle winglets, effectively tip wing extensions, contribute more to the total lift, making the aircraft fly at lower angles of attack, generating a lower induced drag, although with higher root bending moments.

The detailed aerodynamic design of a blended winglet is presented. It is the result of the compromise between induced drag reduction and parasite drag and weight increase. The performance of the aircraft is computed and compared to that of the baseline Falcon 10. Changes in flutter characteristics, fatigue and trim drag are not considered.

The baseline configuration is a Whitcomb-style blended winglet, with a taper ratio of 0.35

and a leading edge sweep angle of 40°. Twelve combinations of cant angle and winglet span were analyzed, using a vortex lattice method (VLM) model, to identify the one providing the best compromise between induced drag reduction and parasite drag and structural weight increase.

For the best winglet, a Reynolds-Averaged Navier--Stokes (RANS) model was created and used to produce drag polars and, thus aerodynamic loads. The loads were the input for a finite element model of the wing box, used to determine the extent of structural reinforcement required and, hence, the weight penalty.

With the new weights and aerodynamics, the range and fuel burn for a typical mission were calculated and compared to the baseline Falcon, establishing the net effect of the winglet.

2 RANS Analysis

A RANS model of the baseline wing was created in ANSYS Fluent® and validated with respect to the wind tunnel data. The winglet was added to that model and the new drag polars and loads were calculated. These data was also used in the calibration of the VLM models.

The wing was modeled with a symmetry boundary condition at the root and an adiabatic, no slip boundary condition at the wing surface. Mach number, static pressure and temperature were imposed at the far field. Air was modeled as an ideal gas, with viscosity set as a function of temperature using Sutherland law and the 2-equation k-ω SST turbulence model, due to its better accuracy in predicting separation.

A grid independence study was performed and validated with respect to the wind tunnel data. Simulations were then run at different angles of attack and Mach numbers. The results were used to calibrate the VLM model in terms of spanwise lift distribution and to derive a friction drag correction factor for the VLM model.

3 VLM Analysis

Due to its quick turnaround time and good accuracy (once it had been calibrated with respect to the wind tunnel data and the RANS model) a VLM model was used to explore the design space, using VLAERO+®. This program incorporates a Prandtl-Glauert compressibility correction.

Once the calibration of the baseline wing model was carried out, the geometry of the winglet 1570 (i.e., 15% span, 70° cant) was created in VLAERO+® and added to the wingtip. With the wing calibrated, the fuselage and engine nacelles were added and calibration of the full VLM model was made to match the wind tunnel results.

Simulations were run for different angles of attack, at Mach 0.7 and Mach 0.8, for the twelve candidate winglet configurations to produce the drag polars for the aircraft with and without winglets.

A separate model was also created to be used in the determination of loads in a sideslip maneuver for the structural analysis.

4 Parasite Drag Model

The winglet parasite drag was calculated using traditional drag buildup methods, i.e., the friction drag of a flat plate of equivalent wetted area, corrected for thickness and sweep through the form factor *FF* and corrected with the RANS results. The friction coefficient C_f is calculated assuming a fully turbulent boundary layer [10].

The total parasite drag of the aircraft with winglets is the drag of the aircraft and wing previously calculated plus the winglet drag, minus the small portion of the wingtip removed for the winglet installation. Interference drag is ignored at this stage but was considered in the full RANS calculation of the final winglet.

5 Winglet Weight

The aircraft empty weight increases because of the winglet itself plus any wing structural reinforcement required by the new loads. The detailed structural design of the winglet was beyond the scope of this work. Therefore, to estimate its weight, a simple model was proposed. McLean [3] quotes the total weight penalty for the 737 NG with API winglets as 300 lb, with 75% being the winglet structure. Also, for the Hawker 800, an aircraft similar in size and mission to the Falcon 10, the total empty weight increase for the aircraft with winglets was reported to be 115 lb [11]. Thus the winglet structure weight for the Falcon 10 is assumed to

be the weight of the Hawker winglet (assumed to be 75% of the total weight penalty reported) scaled by planform area.

6 Structural Reinforcement Weight

Comparison of the stresses imposed by the new loads with the Falcon 10 static stress report [12] was used to determine whether the structural margins in the original structure were sufficient or extra reinforcement was needed.

A finite element model of the wing box was created, validated with respect to the wing box stress analysis report [12] and used for a set of critical loads with the different winglets. The loads were obtained from the VLM models and the new stresses were calculated. Wherever it was necessary to restore positive margins of safety for buckling and, or static strength, stiffeners or doublers were added. The volume of those elements, with the material density and a correction factor (accounting for fasteners) was used to calculate the weight penalty.

The original wing box was sized for two specific load conditions [12]:

1. an upward gust condition, critical for the inboard part of the wing and
2. a roll condition, critical for the outboard section.

An additional loading case was studied, corresponding to a sideslip maneuver because an almost vertical winglet at the tip may result in high bending moments [13]. The maximum gust load factor was found to be the sizing case.

The wing box structure was meshed in ANSYS®, using quad SHELL 181 elements (Fig. 1), with thicknesses matching the geometry in the structural analysis report [12]. The pressure loads came from the VLM models. Inertia loads were applied as distributed forces and the stresses in the wing box were calculated. The spars were fully clamped at the wing root.

Two possible failure modes were considered, panel buckling and tensile failure. The Falcon 10 wingbox material is reported as aluminum A7U4SG-T651. For the structure strength, the maximum and minimum principal stresses were calculated and compared to the material tensile strength. Where the stresses exceeded the allowable values, the skin panels were thickened to reach an 18% margin of safety and the extra weight was calculated.

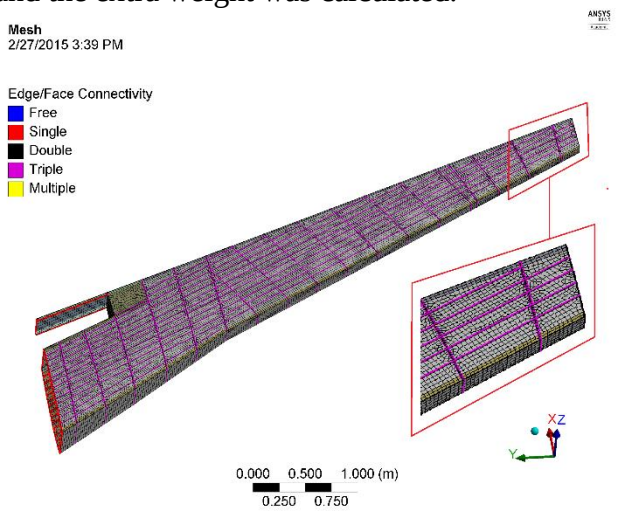

Figure 1. Diagram of the wing box finite element model.

Because of the bending loads, the upper skin is under compression and buckling is likely to occur. The stress report [12] provided test curves for A7U4SG plotting critical buckling stresses as a function of the stiffness parameter $kL\rho$. From these graphs the critical stress value for every panel was determined and compared to the most negative principal stresses from the FEM, at each rib location. When the critical stress was exceeded *Z*-stiffeners were added. The stiffener top flange width was fixed for fasteners installation. The lower flange width and the stiffeners thickness were set as 2.5 times the stiffener height (not to exceed the original wing stiffeners height) and 1.2 times the local skin thickness, respectively. The stiffeners were then sized following the iterative process shown in Figure 2, for an 18% margin of safety. The new stiffeners were placed at the midpoint between the original wing box stiffeners. Their volume was computed and thus the weight was calculated. A 1.5 factor was applied to account for fasteners weight following Niu [14].

7 Winglet Performance Evaluation

For the selection of the best winglet configuration, the winglets net effect on the aircraft range and fuel burn was evaluated. For simplicity, the initial weight was the MTOW and W_1 was set equal to the maximum zero fuel weight plus the winglet and reinforcement

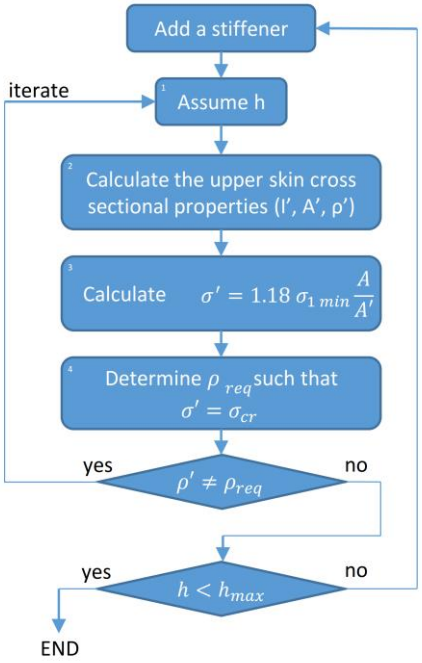

Figure 2. Process followed for stiffener sizing.

weights. The drag polars used were those discussed above.

The specific fuel consumption, *c*, was interpolated for each integration step, from appropriately scaled, published data for the TFE731-1069 engine [15]. The range was calculated for cruise at 35,000 ft and 40,000 ft altitudes at Mach 0.7 and 0.8.

The net benefit was measured by the change in range and fuel burn for the entire NBAA mission because, for medium range aircraft, a significant portion of the flight time is spent in climb.

For simplicity, the amount of fuel for reserves at the end of the mission was assumed to be the same for both aircraft (baseline and with winglets). For all cases the aircraft took off at MTOW, from sea level, carrying a crew of 2 (170 lb each) and 4 passengers (165 lb each).

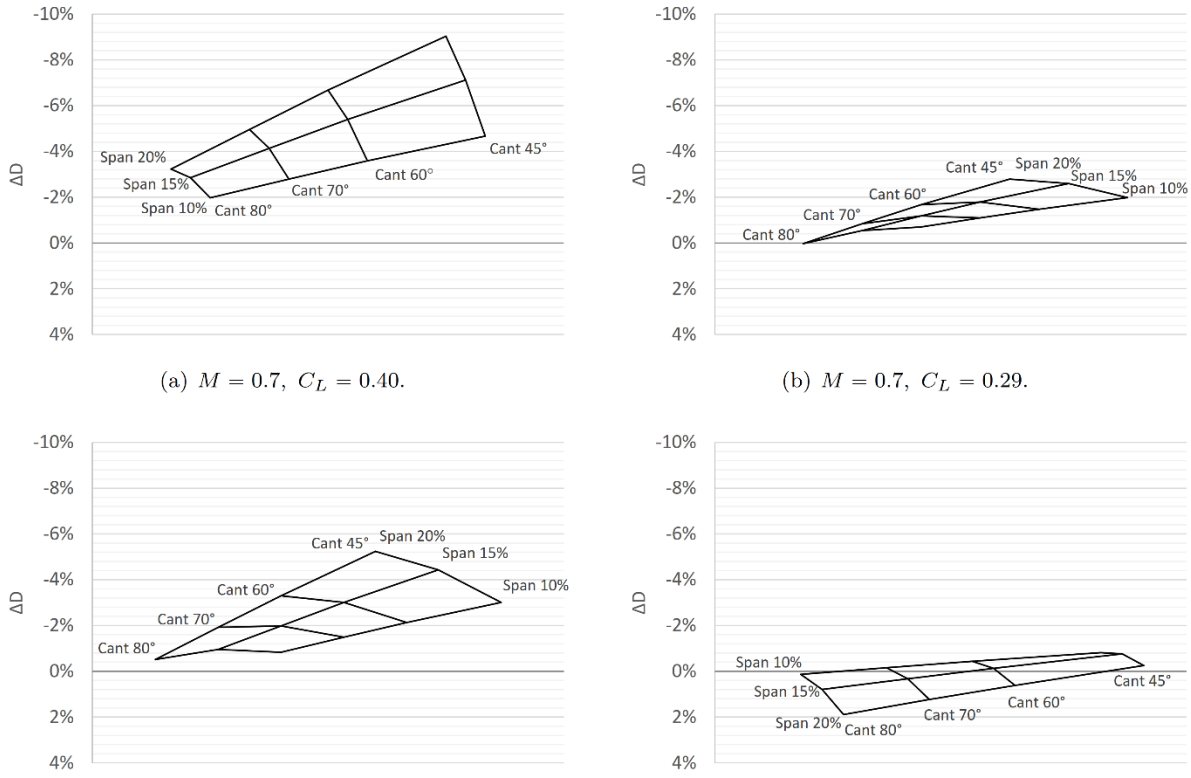

(a) $M = 0.7,\ C_L = 0.40.$ (b) $M = 0.7,\ C_L = 0.29.$

(c) $M = 0.8,\ C_L = 0.32.$ (d) $M = 0.8,\ C_L = 0.25.$

Figure 3. Total drag change with respect due to winglet span and cant angle for given Mach and lift coefficients.

8 Results

8.1 Winglets Effect on Total Aircraft Drag

Figure 3 presents the total drag change as a function of winglet span and cant angle, for lift coefficients representative of the top of climb and top of descent conditions.

The most significant changes occur at Mach 0.7, top of climb (highest C_L and, thus, highest induced drag). Conversely, at the end of cruise, for Mach 0.8, the net aerodynamic effect is detrimental (Fig. 3 (d)). Here the induced drag reduction is exceeded by the parasitic drag increase brought about by the larger wetted area.

The data shows that lower cant angles give larger drag reductions, thus favoring planar wingtip extensions. However, from the global effect on the aircraft, that conclusion is incomplete because it lacks the weight penalty induced by the changes in bending moments.

8.2 Weight Increase

The critical case sizing the inboard wing with winglets is the gust condition, same as for the original wing [12]. However, for the outboard wing, with winglets, the critical case changes from the roll to the sideslip maneuver.

Dassault static stress data [12] indicates that the inboard section was constructed with higher structural margins and, therefore, does not require extra reinforcement. The maximum principal stresses in the upper skin display relatively high margins of safety with respect to the material ultimate tensile strength for the 10% and 15% span winglets. Only the 20% span winglets required minor skin reinforcement between ribs 15 and 16 for static strength in the sideslip maneuver case.

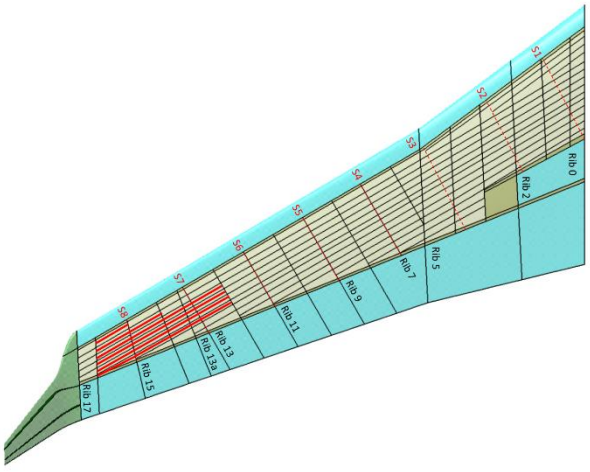

Figure 4. Extent of the wing box reinforcement needed for winglet 1545.

The FEM shows panel buckling as the predominant failure mode for the sideslip maneuver case. Figure 4 highlights, for winglet 1545, the region in the outboard wing where extra stiffeners were added to prevent buckling.

The weights of the winglet and the wing reinforcement, for each winglet configuration, are presented in Fig. 5. As expected, larger winglet spans and greater cant angles require heavier reinforcements, since the winglet present a greater normal area to the flow in sideslip, hence inducing larger bending moments.

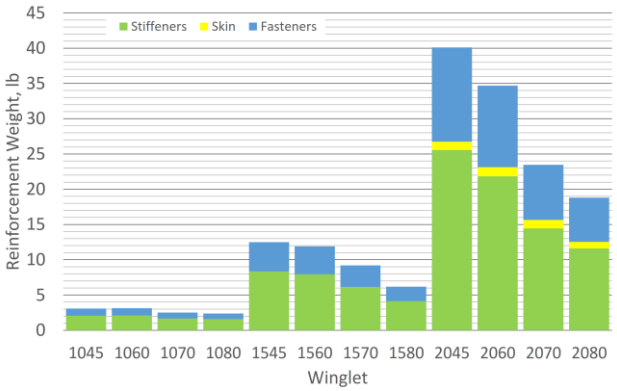

Figure 5. Winglet configurations weight penalties.

8.3 Winglet Configuration Effect on Range

Figure 6 presents the change in range as a function of winglet span and cant angle. Comparison of Figs. 3 and 6 show some similar trends but with. a few significant differences. While the largest winglets give the highest induced drag reduction, they do not necessarily provide the highest range increase. For example, winglet 2045 outperforms the other winglets at Mach 0.7, 40,000 ft, but it is not better than winglet 1545 for the other cruise conditions evaluated. Furthermore, it becomes detrimental at Mach 0.8, 35,000 ft, while winglet 1545 is almost neutral for that case.

It was also shown in Fig. 5 that winglet 2045 would require extensive reinforcement, something that would significantly increase the installation costs. Therefore, winglet 1545 (Fig. 7) was considered the best configuration.

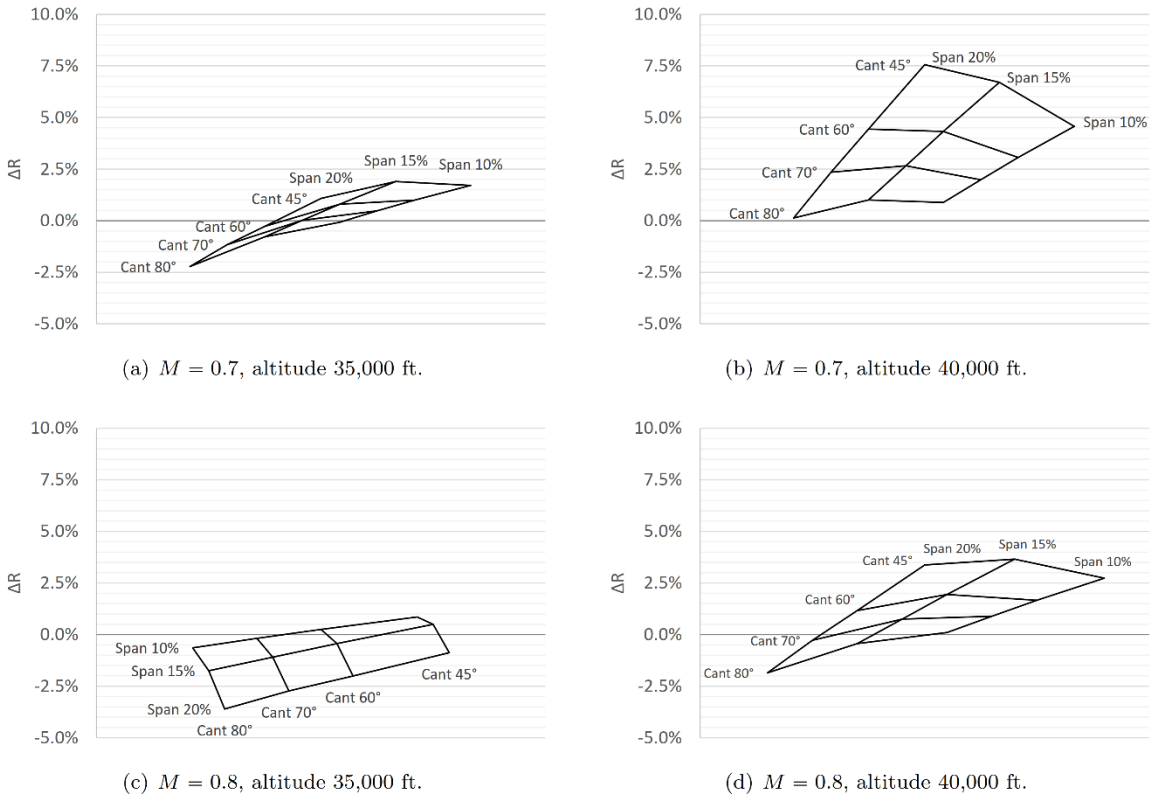

Figure 6. Change in range as a function of winglet span and cant angle for cruise at constant Mach and altitude.

8.4 Winglet 1545 Aerodynamics

Detailed RANS analysis was conducted at Mach 0.7 and 0.8, for a range of angles of attack, to generate accurate drag polars and to examine whether any compressibility issues, such as shock waves, were present that would require a winglet redesign.

Figures 8 and 9 show the computed lift curve and drag polars for the baseline wing with and without winglet, together with the wind tunnel data[1]. The induced drag curves show very good agreement.

Figure 11 shows pressure coefficient contours, streamlines, shock waves (in red) and tip vortex cores (in green) and it indicates that shock waves or separation do not occur on the winglet until after they had already appeared on the baseline wing.

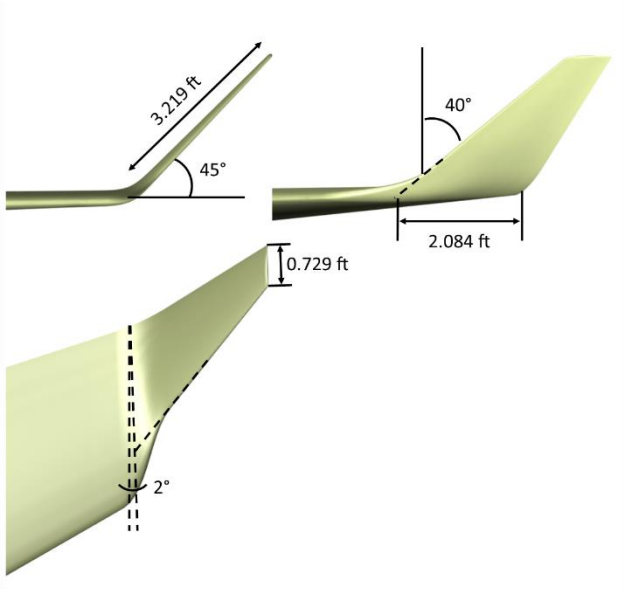

Figure 7. Winglet 1545 geometry (15% span, 45° cant angle).

[1] The wind tunnel data correspond to the tail-off aircraft, whereas the CFD calculations are for the wing only.

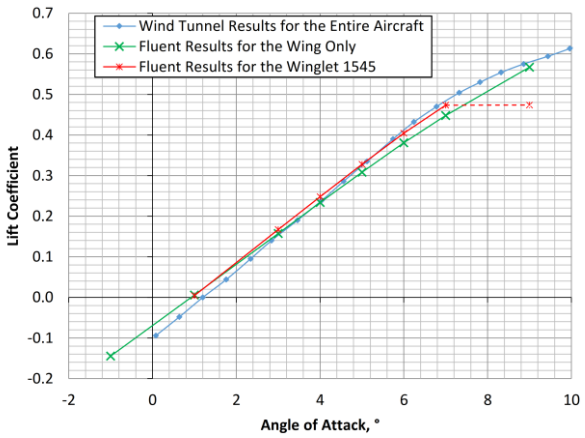

Figure 8. Lift coefficients vs. angle of attack at Mach 0.7 for wing with and without winglet.

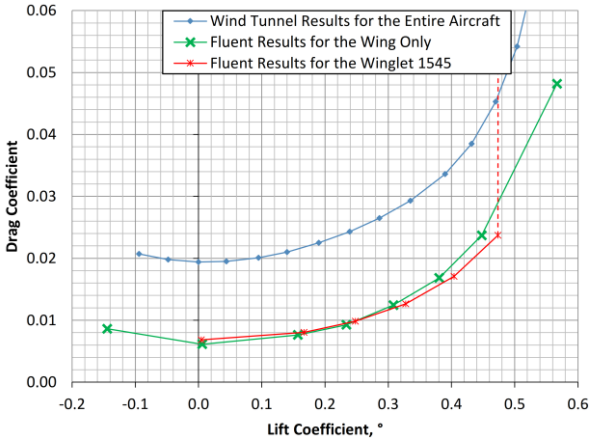

Figure 9. Drag polar at Mach 0.77 for wing with and without winglet. Includes tail off aircraft wind tunnel data. Calculations are RANS.

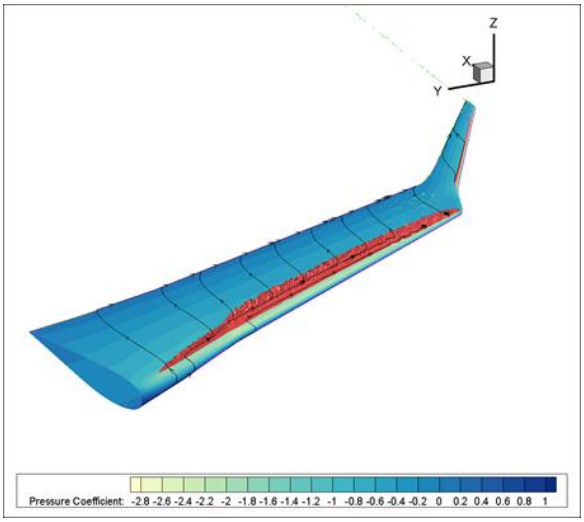

Figure 10. Pressure contours from RANS for wing with winglet 1545 at Mach 0.7, α = 7°

8.5 Full Mission Analysis

The range and fuel burn were recalculated for this winglet using the aerodynamic data presented above. The results are summarized in Fig. 11.

The best range improvement was found to be 101 NM, i.e. 7.0% of the original value, for a cruise at Mach 0.7 at 40,000 ft. However, it is unlikely that the aircraft would cruise at 40,000 ft when taking off at MTOW because that altitude is close to the aircraft operating ceiling.

For a cruise at Mach 0.8 and 40,000 ft the winglet increases the range by 4.4%. For a cruise at 35,000 ft, the winglet slightly improves the aircraft range.

The best total range is accomplished at Mach 0.7 and 35,000ft.

The fuel burn for a 1,200 NM mission is presented in Fig. 11 (b) where it can be seen that 8% savings are provided.

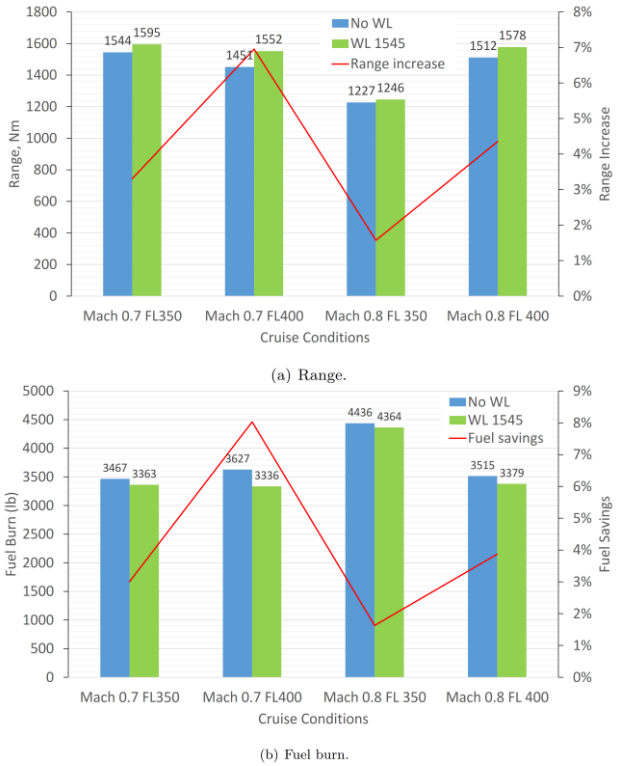

Figure 11. Mission analysis results.

9 Conclusions

1. The preliminary design of a Whitcomb-style winglet for the Dassault Falcon 10 was conducted using VLM, RANS computational fluid dynamics and FEM for determining the necessary structural reinforcement. The models were fully validated with respect to experimental data provided by Dassault.

2. A design space constituted by the set of twelve winglet with spans between 10 and 20% and cant angles between 45 and 80° was explored using VLM. The configuration providing the greatest net benefit was 15% in span (i.e., 3.2 ft) with 45° of cant, being the compromise between induced drag reduction and profile drag and structural weight increases due to larger spans (i.e., greater wetted areas).

3. For the winglet mentioned above, at typical cruise lift coefficients, the net drag reduction was 4.8% at Mach 0.7 and 2.5% at Mach 0.8 and the weight increase was estimated to be 127 lb. When the aerodynamic and weight effects are taken into consideration, for a typical mission (Mach 0.8 cruise at 40,000 ft and carrying 4 passengers with a crew of 2), the range was increased by 66 NM (4.3%). For a 1,200 NM mission, at Mach 0.8 and 40,000ft altitude, fuel burn is reduced by 3.9%. The maximum range was increased by 3.3% and the minimum fuel burn was reduced by 3.8%. The maximum proportional improvements in range and fuel burn were 7 and 8%, respectively.

4. VLM models were efficient at the winglet geometry selection stage. However, for the accurate estimation of the winglet global effect RANS was necessary because it includes viscous effects and compressibility. The RANS model showed that the design did not present any detrimental compressibility effects such as shock waves or separation.

5. Whereas for the original wing, for the outboard section, the critical loading case was the roll maneuver, the FEM revealed that the sizing case for the wing with a winglet was the sideslip maneuver. The gust condition is critical for the inboard wing, with and without winglets. However, for the Falcon 10, no extra reinforcement was necessary because the original wing box possessed substantial structural margins.

6. This work has shown the potential gains that a retrofit winglet would bring to the Falcon 10. Next phase of work should focus on the design of the winglet structure, including factors such as flutter and fatigue. Other areas requiring further exploration are the effects of the winglet on the aircraft stability and control, on trim drag and its interaction with the control surfaces. All, both at altitude and in ground effect.

Figure 12. Artist impression of Falcon 10 with winglet 1545.

Acknowledgments

The authors would like to express their gratitude towards Dassault Falcon Jet and Dassault Aviation for the financial and technical support of this project.

References

[1] Anon., *Falcon 10 Operational instructions manual*, Avions Marcel Dassault-Breguet Aviation, 1993, Revision 12.

[2] Falcon 10/100 Census, Retrieved March 2015, from Jet Photos: http://www.jetphotos.net/census/index.php, 2015.

[3] McLean, D., Wingtip devices: what they do and how they do it, *Performance and Flight Operations Engineering Conference*, 2005.

[4] Whitcomb, R. T., A design approach and selected wind-tunnel results at high subsonic speeds for wing-tip mounted winglets, NASA, TN-D-8260, 1976.

[5] Mann, A., The modelling and design of advanced wing tip devices, Aeronautics Days in Vienna, 2006.

[6] Kroo, I., Nonplanar wing concepts for increased aircraft efficiency, VKI lecture series on innovative configurations and advanced concepts for future civil aircraft, 2005.

[7] Poisson-Quinton, P., Parasitic and interference drag prediction and reduction, *Aircraft Drag Prediction and Reduction*, 1985.

[8] Spillman, J., The use of wing tip sails to reduce vortex drag, *Aeronautical Journal*, 1978, pp. 387 - 395.

[9] Takenaka, K., Hatanaka, K., Yamazaki, W., and Nakahashi, K., Multidisciplinary design exploration for a winglet, *Journal of Aircraft*, Vol. 45, No. 5, 2008.

[10] Bertin, J. J. and Cummings, R. M., *Aerodynamics for Engineers*, Pearson, Boston, Mass, 2014.

[11] Anon., Hawker 800SP & Hawker 800XP2, Retrieved December 2014, from Aviation Partners Inc.: http://www.aviationpartners.com/hawker.html, 2014.

[12] Avions Marcel Dassault - Breguet Aviation, Falcon 10 serie, *Calcul de la voilure premiere partie*, Avions Marcel Dassault Technical Report.

[13] Faye, R., Laprete, R., and Winter, M., Blended winglets for improved aircraft performance, *Aero Magazine*, No. 17, Boeing, 2002, pp. 16 - 31.

[14] Niu, M. C. Y., *Airframe stress analysis and sizing*, Conmilit Press Ltd., Los Angeles, Calif; Hong Kong, 2nd ed., 1999.

[15] Nicolai, L. M. and Carichner, G., *Fundamentals of aircraft and airship design*, American Institute of Aeronautics and Astronautics, Reston, VA, 2010.

Copyright Statement